Acta Astronautica 169 (2020) 170–179

Contents lists available at ScienceDirect

Acta Astronautica

journal homepage: www.elsevier.com/locate/actaastro

Research paper

Damping device to reduce the risk of injection-coupled combustion instabilities in liquid propellant rocket engines

Wolfgang Armbruster[a,*], Justin S. Hardi[a], Yannik Miene[a], Dmitry Suslov[a], Michael Oschwald[a,b]

[a] Institute of Space Propulsion, DLR, Hardthausen, Germany
[b] Institute of Jet Propulsion and Turbomachinery, RWTH Aachen University, Aachen, Germany

ARTICLE INFO

Keywords:
Liquid propellant rocket engine
Combustion instability
Injector coupling
Damping device

ABSTRACT

A new countermeasure against injection-coupled combustion instabilities in liquid propellant rocket engines is presented. Whereas the problem is usually addressed by adding damping elements such as baffles or resonators to the combustion chamber, this approach directly damps the acoustic eigenmodes of the injector instead. The principle of the damping method is described in this article, as well as the implementation of such a device in a sub-scale rocket thrust chamber operated with liquid oxygen and hydrogen at conditions representative of upper stage engines. Test results are presented which show that flame and pressure oscillations were successfully reduced by the modification. The absorbers had no measurable influence on thrust chamber performance, and so the solution lends itself to retrofitting in existing engines, as well as integration during the design phase.

1. Introduction

Since the development of the first large liquid propellant rocket engines (LPRE) high-frequency combustion instabilities have been one of the major challenges facing designers [1]. A well-known example of the occurrence and costly resolution of combustion instabilities is the development of the F-1 engine [2]. The underlying coupling mechanisms leading to instabilities are still not fully understood [1]. Thus, even some of the latest engines have suffered from instabilities during development, for example the Japanese LE-9 [3].

Other recent examples of rocket engines using different kind of propellants and suffering from combustion instabilities can be found in the Japanese engine LE-5B [4], the Chinese YF-100 [5], a predecessor of the European Aestus called L7 [6], the Aestus engine itself [7] and the HM7 [8]. Also several cryogenic research combustors using shear coaxial injection elements of different scale and representativity showed high-frequency combustion instabilities for the propellant combination liquid oxygen - hydrogen (LOX/H_2) [9,10] and LOX/CH_4 [11–13]. Due to the extreme power density in rocket combustors, only a small fraction of the total heat release needs to be transferred into the acoustic field to get rapidly growing amplitudes which can lead to the destruction of the engine by increased mechanical and thermal loads on the walls [14]. In general, combustion instabilities are driven by thermoacoustic interaction: the pressure amplitudes increase if unsteady heat release is in phase with the pressure oscillation. The Rayleigh criterion used to evaluate energy transfer into the acoustic field is based on this principle [15]. In a real system with acoustic dissipation, the energy transfer from combustion into the acoustic field must overcome the damping of the system in order to excite combustion instabilities. This balance can be described by Eq. (1), where L_i represents the i_{th} damping process [16,17].

$$\int_0^T \int_V p'(x,t)\dot{q}(x,t)\mathrm{d}V\mathrm{d}t > \int_0^T \int_V \sum_i L_i(x,t)\mathrm{d}V\mathrm{d}t. \tag{1}$$

According to Eq. (1), there are two possibilities to increase the stability margin in a rocket engine. One can either try to reduce the combustion response and hence the driving source of the system, for example by varying the injector design, or one can increase the damping in the chamber, so that it exceeds the energy gain from combustion [1]. The driving mechanisms are often difficult to be identified, and so the most common approach to eliminate combustion instabilities is to add acoustic damping features to the combustion chamber.

2. State-of-the-art damping devices in rocket engines

Although extensive effort was put into investigating damping methods during the past decades, practical damping devices used in liquid propellant rocket engines are effectively unchanged. The main devices are baffles extending into the combustion chamber volume, or

* Corresponding author. .
E-mail address: Wolfgang.Armbruster@dlr.de (W. Armbruster).

https://doi.org/10.1016/j.actaastro.2019.11.040
Received 29 October 2019; Received in revised form 19 November 2019; Accepted 24 November 2019
Available online 15 January 2020

Nomenclature

A	area, m^2
c	speed of sound, m/s
$c*$	characteristic velocity, m/s
f	frequency, Hz
I	intensity of PM signal, V
l	length, m
$\dot{m}$	mass flow, kg/s
p	pressure, bar
$\dot{q}$	volumetric heat release rate, W/m^3
t	time, s
T	period, s
u	velocity, m/s
V	volume, m^3
ζ	pressure loss coefficient

Subscripts

cc	combustion chamber
exp	experimental
inj	injector
HR	Helmholtz resonator
t	nozzle throat

Abbreviations

BKD	Research combustor model "D″
DLR	German Aerospace Center
LOX	Liquid Oxygen
LP	Load Point
LPRE	Liquid Propellant Rocket Engine
PM	Photomultiplier
PSD	Power Spectral Density
ROF	Ratio Oxidizer to Fuel
SLM	Selective Laser Melting

acoustic resonators connected to the chamber wall. The implementation of baffles and absorbers (here as an acoustic liner) are illustrated conceptually in Fig. 1, and their drawbacks are discussed in the following sections.

2.1. Baffles

Baffles are walls emerging from the injector faceplate into the combustion chamber. Sometimes also certain injectors with increased length were used in the past as damping baffles, instead of additional walls. The purpose of the baffle is to disturb acoustic mode symmetries in the combustion chamber and to dissipate acoustic energy through interaction with the velocity field. In the aforementioned example of the F-1 engine, about 2000 full-scale tests with 15 different baffle configurations were necessary to find a stable solution.

Other prominent examples in the United States with baffles include the Space Shuttle Main Engine (SSME) [14,18], the M − 1 engine, the Chinese YF-77 [19], the Japanese LE-7 [14], and the Russian RD-170 and its derivatives [20]. The gas generator of the European Vulcain is also stabilized with baffles [20].

Although baffles have been used for decades, their damping processes are still not fully understood [6]. Thus baffle design usually relies on trial-and-error with expensive full-scale engine tests. Other drawbacks of baffles are.

- cooling requirements [1,14],
- increased engine weight,
- a possible reduction in performance [1],
- ineffective damping of longitudinal modes [1], and
- usually negligible damping of higher order transverse modes [1,21].

2.2. Resonators

Other common damping devices for LPREs are acoustic resonators of the Helmholtz or quarter-wave types. Usually the resonators are placed close to the faceplate between the injector head and the cylindrical chamber wall, as can be seen in the Vulcain 2 thrust chamber in Fig. 2.

Other examples of rocket engines using acoustic resonators are the RL-10 [14] and SSME in the US, the European L7 engine [6], and the LE-5 [20], LE-7 [4] and LE-9 [3]engines in Japan.

An advantage of acoustic resonators compared to baffles is that the damping characteristics can be modelled quite accurately. Thus the absorbers can be tuned to certain chamber frequencies and their design is based less on empirical data than baffles. The resonant frequency of a Helmholtz resonator can be estimated by Eq. (2)

$$f_{HR} = \frac{c}{2\pi}\sqrt{\frac{A}{V(l+\Delta l)}}, \tag{2}$$

where A is the orifice area, V the volume of the resonator cavity and l the orifice length, which is often corrected by Δl with a value usually around $0.85d$ [21].

A complication is the prediction of the speed of sound in the cavities. Since many processes such as injection, atomization, mixing, combustion, and recirculation of combustion products take place in the vicinity of the cavity inlets, the gas composition and temperature, and therefore the speed of sound, are not well defined at this location. Therefore accurate tuning of the absorbers requires high-fidelity

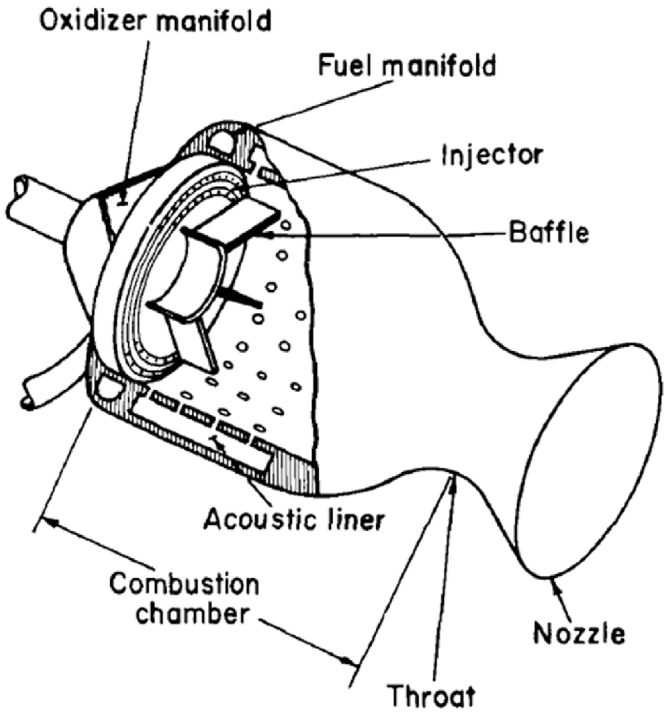

Fig. 1. Acoustic damping devices in rocket combustion chambers [1].

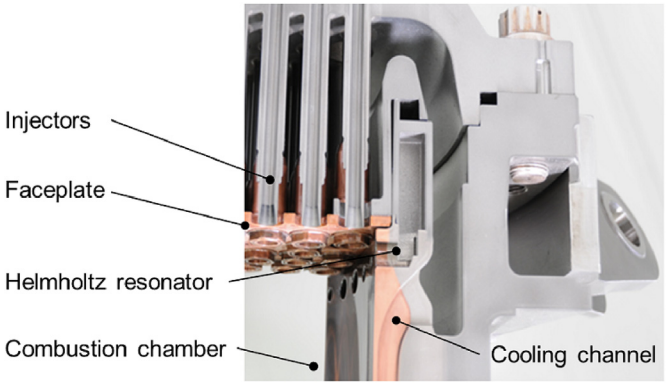

Fig. 2. Helmholtz resonator of Vulcain combustion chamber. Courtesy of ArianeGroup.

simulations or expensive full-scale testing. Furthermore, it is unlikely that chamber and resonator acoustics are affected by operating conditions changes in a proportional manner. For that reason, the resonators can only be optimally tuned for a certain load point. In summary, the main drawbacks of chamber absorbers are.

- complexity of chamber wall cooling at absorber locations,
- difficulty in estimating the speed of sound in the cavity,
- and optimal tuning only for one defined load point.

2.3. Injector detuning

For injection-coupled instabilities, damping combustion chamber acoustics does not address the mechanism driving the instability, only the resulting chamber pressure oscillations. Injection coupling is described as the interaction of fluctuations in the injectors with the pressure oscillations in the combustion chamber [22]. It has been identified to lead to combustion instabilities in cryogenic rocket engines with coaxial injectors, from research experiments [9,11,13] to full-scale engines [3,22]. The principle is illustrated well by the recent work of Gröning et al. [10]. Self-excited high-frequency combustion instability of the first tangential (1T) chamber resonance mode was observed in a sub-scale research thrust chamber [10,23].

One strategy for counteracting injection-coupling is changing the injector length to decouple injector and chamber acoustics. In Russian rocket engines a similar approach is called “adjusted injectors” [20]. While this effectively disrupts the driving mechanism of the instability, it can be very costly to modify the injectors late in engine development. Furthermore, experience with the LE-9 engine showed that even the change of injector design could not fully stabilize the combustion and conventional acoustic dampers in the combustion chamber were still necessary [3].

3. Concept and design of new damping device

3.1. Basic principle of the damping device

Usually combustion instabilities are damped by resonators connected to the combustion chamber, which comes with several drawbacks, as summarized in Section 2. However, since for the investigated research combustion chamber the instabilities’ coupling mechanism was identified as injection-coupled, it is also feasible to reduce the driving, as can be seen in Eq. (1).

The new damping device presented in this work was motivated by the hypothesis that damping the injector eigenmodes would eliminate a common driving source for combustion instability, especially for injection coupling.

The device, therefore, essentially connects an acoustic damping cavity to the inner volume of the injection elements. By doing so, the amplitude of longitudinal resonance modes of the injectors which lead to heat release oscillations should be reduced. Fig. 3 illustrates the principle of the damped injectors for a simplified rocket combustion chamber configuration.

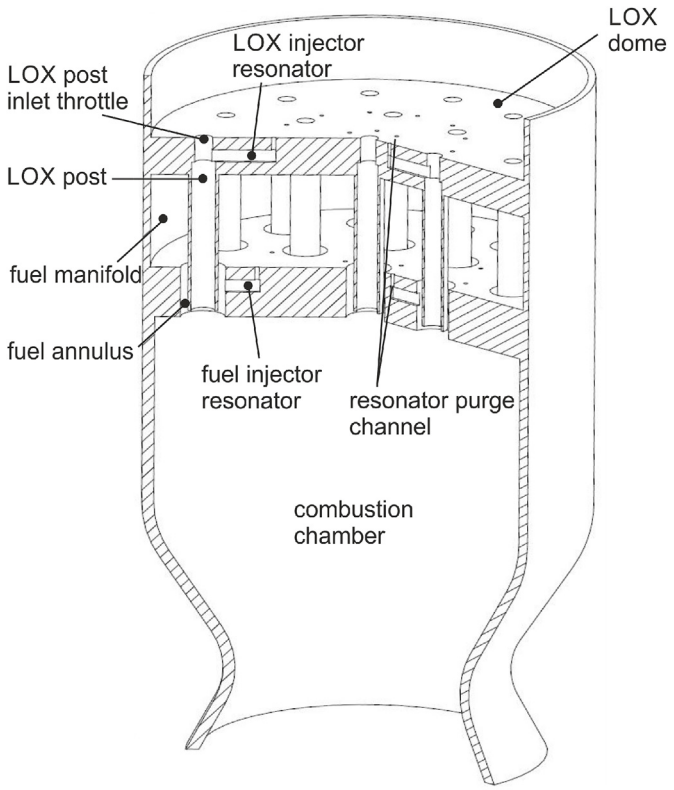

Fig. 3. Sketch of the basic principle of the new damping device.

The cavities are purged with the propellant from the upstream distribution manifold to fill them with the same media with nearly the same state (pressure, temperature) as in the injector itself, and avoiding the problem of undefined gas conditions facing resonator elements in the combustion chamber. Tuning of the cavity to longitudinal eigenmodes of the injector is thereby independent of the speed of sound and is a purely geometrical problem, as indicated in Eq. (3).

$$\begin{aligned} f_{inj} &= f_{HR} \\ n\frac{c_{LOX}}{2(l_{inj}+\Delta l)} &= \frac{c_{LOX}}{2\pi}\sqrt{\frac{A}{V(l+\Delta l)}} \\ f_{inj}(l_{inj}) &= f_{HR}(A, V, l) \end{aligned} \tag{3}$$

In the case of a quarter-wave absorbers the geometrical relation would simply lead to a length ratio of absorber to injector tube length, e.g. for damping the second longitudinal (2L) eigenmode of the injector the cavity length would be 1/4 of the post length. Helmholtz resonators have been chosen over quarter-wave absorbers because they can be more compact and have broader absorption characteristics [24].

3.1.1. Advantages of this damping method

The purging concept for the resonator is considered to be an important feature. The purging channel connecting the resonator volume with the injector manifold determines that the resonator volume is filled with the same fluid as the injector itself. Temperature changes in the injector head and the pressure loss in the Helmholtz resonator neck can be considered negligible. This means the same fluid with the same density and speed of sound is in the resonator as in the injector itself. Any change in propellant state resulting in a shift in injector mode frequencies will result in a corresponding shift in the resonator damping

frequency. Therefore, the resonator can be said to be tuned to the injector and not only to a particular operating condition.

The independence of speed of sound of the medium allows the damping characteristics to be verified with cold-flow tests of the injector head or with hot-fire tests of a single injector element. This drastically reduces cost and time compared to the necessary full-scale tests for chamber wall resonators or baffles. Due to the location of the resonators within the injector head, adjustments of the cooling is not required. For that reason, the absorbers could be retrofitted to an engine with relative ease after instabilities with injection-coupling arise. The late integration should be especially easy for additively manufactured injector heads.

The location of the resonators at the post inlet is not expected to impact the injection conditions at the injector exit. Therefore, the resonators have theoretically no influence on the performance of the engine with respect to combustion efficiency. The inlet throttle orifice diameter can be adjusted so that the combination of LOX inlet resonator purge flow and pressure drop match that of the undamped injectors.

Injector heads of LPREs contain a large number of injection elements, typically several hundred. If necessary, several different resonator geometries can be realized in the injector head in order to damp different injector mode frequencies which could couple with various chamber modes.

In summary, key engine parameters such as injector pressure drop, performance and mass are theoretically not influenced by this damping device, and compared to baffles or resonators in the chamber, tuning of the dampers can easily be calculated and is valid for all operating conditions. Verification of the damping characteristics should be relatively inexpensive.

3.1.2. Limitations of this damping method

The following limitations of this damping method have been identified. First, its applicability is limited to rocket engines with an identified injection-coupling instability mechanism. It is unclear if the injector damping would help stabilize instabilities driven by other mechanisms.

So far the damped injectors have only been verified for shear coaxial injector elements with the propellant combination LOX/H_2, as will be presented in this work. Nevertheless, the operating principle is expected to be valid for coaxial injectors using other propellant combinations.

4. Experimental verification

4.1. Intergration with DLR research combustor D (BKD)

4.1.1. Combustor D (BKD)

The new damping device was tested on the DLR research thrust chamber model “D” (BKD). BKD is a cryogenic, sub-scale rocket thrust chamber, which has been used with the propellant combinations LOX/H_2 and LOX/CH_4 for various research topics. In past LOX/H_2 campaigns it was observed that self-excited high-frequency combustion instabilities appeared for certain load points [10].

Five test campaigns to analyze the coupling mechanism of the instability have been undertaken at the European Research test bench for cryogenic high pressure combustion P8 from 2011 until today. The latest configuration for stability investigation, as shown in Fig. 4, consists of three main elements: injector head, cylindrical combustion chamber segment and nozzle segment. For the investigation of combustion instabilities, an instrumented measurement ring is mounted between the injector head and the cylindrical segment. Although a subscale thrust chamber, the experiment is representative of industrial engines in terms of its characteristic chamber length (L* = 0.66 m), contraction ratio (2.56), and multi-element injector head with 42 shear coaxial injection elements.

4.1.2. Instability coupling mechanism in BKD

Self-excited high-frequency combustion instability of the first tangential (1T) chamber resonance mode around 10 kHz was observed for the operating condition of a static combustion chamber pressure of p_{cc} = 80 bar, a propellant mixture ratio of (ROF = $\dot{m}_{O2}/\dot{m}_{H2}$) ROF = 6 and a hydrogen injection temperature of T_{H2} = 95 K [10,23]. Fig. 5 shows a chamber pressure oscillation spectrogram for a typical test sequence.

Gröning et al. [10] used optical probes to record fluctuating OH* radiation intensity of individual flames. The signals revealed that dominant frequencies in the unsteady combustion correspond to LOX injector modes, rather than chamber acoustic modes. As can be seen in the OH* spectrogram in Fig. 6, the dominant LOX injector mode lines are present for both stable and unstable conditions and do not follow the evolution of chamber mode frequencies.

For that reason, Gröning et al. described the coupling mechanism as injection-driven [26]; the flames are continually modulated by the LOX post acoustics, and the combustion instabilities occur when the frequency of the chamber 1T mode matches one of the longitudinal modes (2L in this case) of the LOX post [10]. This mechanism was later confirmed with high-speed imaging of the flame dynamics in the thrust chamber using the optical access window in the measurement ring [25].

4.1.3. Damper distribution in the experiment

The new damping device was implemented in BKD to damp acoustic modes in the oxygen injectors. The fuel side of the injectors remained unchanged within the scope of this study. Access to the LOX posts was most easily achieved by exchanging the throttle plate with a version including the resonators. This throttle plate defines the geometry of the pressure-drop orifices at the inlets to the injectors, and can be exchanged without affecting any other part of the injector head. Fig. 7 illustrates the principle of the damped injector throttle in comparison to a standard injector.

It should be noted that the principle of the damping device does not require the placement of absorbers at the location of the throttle. It would also be effective if connected to the LOX post elsewhere, provided the location coincides with a pressure antinode of the acoustic mode to be damped. The injector pattern of the experiment consists of 42 injection elements in three rows, as can be seen in Fig. 11. The main coupling is between the LOX post 2L and chamber 1T mode. Additionally, the post 3L mode can interact with the chamber 2T mode,

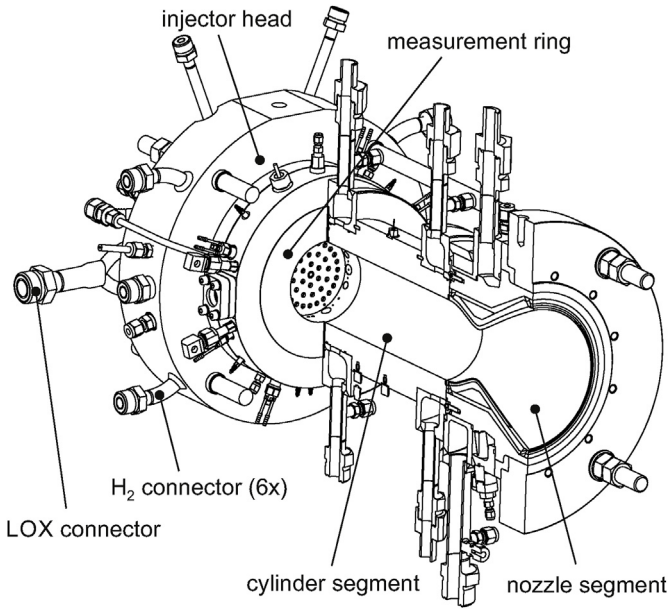

Fig. 4. DLR research combustor model “D” (BKD).

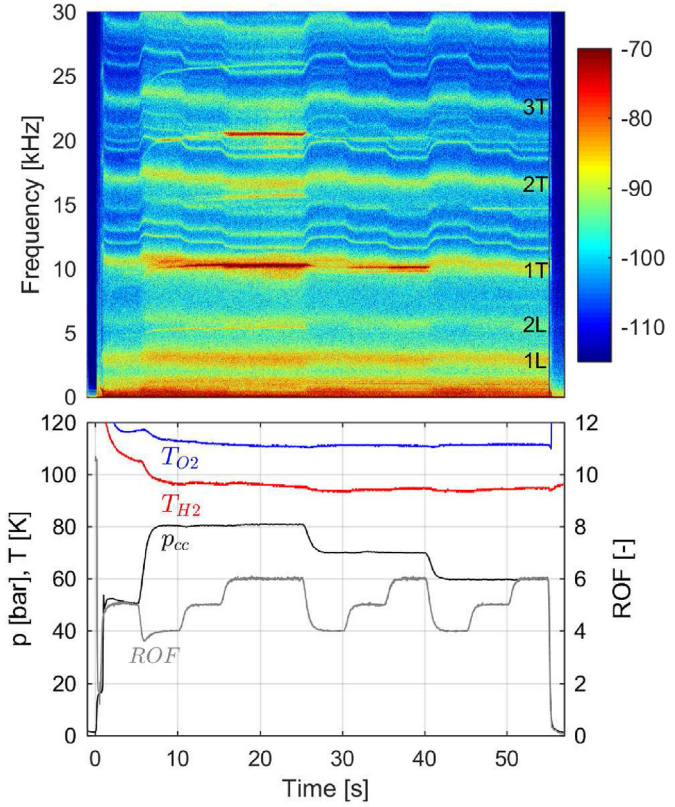

Fig. 5. Pressure oscillation spectrogram over test sequence for a typical test run with standard injectors [25].

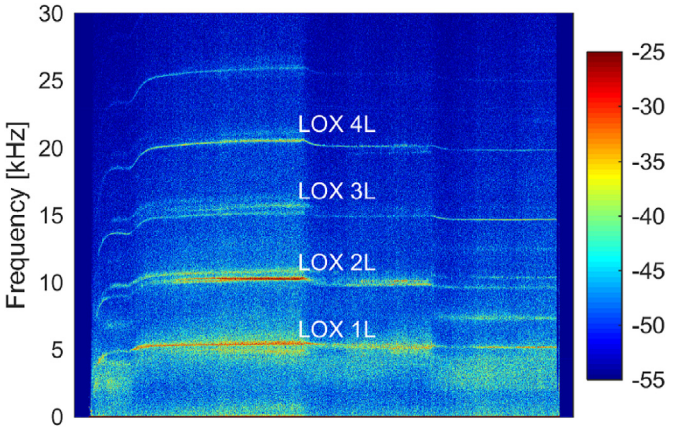

Fig. 6. OH* spectrogram for the test run presented in Fig. 5.

and the LOX 4L with the chamber 1R [26]. The fundamental mode of the injectors (1L) has never been observed to couple with chamber acoustics. For that reason, it was decided to attempt to dampen the injector modes connected to instabilities; namely 2L, 3L, and 4L.

The dampers in the outer row were tuned to the LOX post 2L mode. The dampers of the 12 middle ring injectors were tuned to the post 3L, and the six remaining injectors of the inner row to the post 4L. Due to uncertainties of the resonator design geometries in the manufacturing process, and the limited space in the throttle plate, four different resonator geometries were designed for the outer row and two for the middle row, as summarized in Table 1.

Two injectors of the outer row have the standard throttle without dampers in order to have a direct comparison of the flame dynamics in the same test at exactly the same conditions. The probe PM1 is directed at the flame of a damped inner row injector, and PM3 and PM4 are

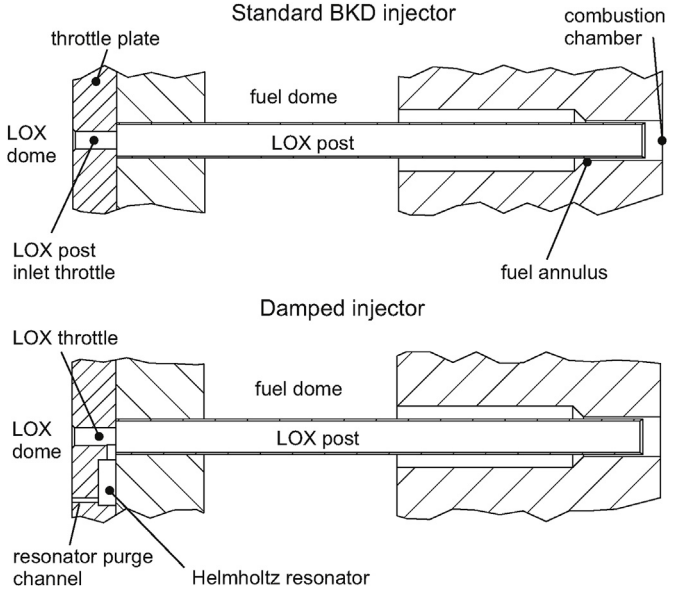

Fig. 7. Drawing of standard BKD injector element and acoustically damped LOX injector.

directed at outer row injectors which are tuned to damp the 2L post mode (10 kHz). For comparison, PM2 is aligned with one of the two undamped injectors of the outer row.

4.1.4. Detailed design of resonators

The frequency of Helmholtz resonators (Eq. (2)) is not valid for resonator volumes with an additional purging channel. Furthermore, connecting acoustic dampers to the LOX posts will also shift frequencies of the injectors themselves. Therefore, Eq. (2) has only been used for preliminary dimensioning of the resonators.

The diameter of the purging flow channels, connecting the LOX dome with the resonators, was fixed early in the design process. The purging holes should allow a small flow of propellants to achieve the same properties as in the injectors, but be as small as possible to minimize the effect on the resonance mode of the Helmholtz resonator. A diameter of 0.4 mm was chosen. The channel connecting the resonator volume with the injector, was defined as a square channel with 0.25 mm^2.

Detailed resonator tuning was then performed with acoustic modelling in COMSOL multiphysics. The main focus was to get the respective resonance frequency of the injector post to coincide with the resonator. With the geometrical boundaries already given, the resonator volume and the length of the neck channel had to be optimized. An acoustic model was created in the pressure acoustics interface, which solves the wave equation in the frequency domain.

The LOX was modelled as a linear-elastic fluid and the properties were calculated with REFRPOP 9.1 [27]. Since the tuning of the post and resonator should by its definition be independent of the LOX properties, constant values of typical BKD conditions (ρ = 1050 kg/m^3, c = 780 m/s) were used.

Although the geometry would allow using symmetry, a full 3D

Table 1
Realized damper distribution.

Injector row	outer	middle	inner
Number of injectors	24	12	6
Resonators tuned to LOX post	2L	3L	4L
Potentially driven chamber mode	1T	2T	1R
Approx. frequency of dampers [kHz]	10	15	20
Damper design variations	4	2	1

approach was chosen. The unstructured tetrahedral mesh had around 10,000 elements for the different resonators. A mesh convergence study has been conducted for one of the cases and a further refinement of the mesh changed the resonance frequency by less than 0.5%. However, the relative frequency difference between the resonator and post did not change with further refinement of the mesh.

Due to low Mach numbers in the LOX injectors, use of the Helmholtz solver was justified. The throttle and purging inlet, as well as the exit into the combustion chamber, were treated as sound-soft (open) boundaries. This simplification can be justified by the previous investigation of LOX post mode shapes and matches the experimental observations [26]. Several parametric sweeps were performed varying the length, width, and height of the resonator. The optimal resonator geometry was chosen for the smallest frequency spacing between the longitudinal mode in the post and the resonator mode.

Fig. 8 shows an exemplary result of the acoustic pressure distribution for the LOX post 2L mode frequency with a tuned Helmholtz resonator connected to the inlet throttle. For visualization the 3D solution was cut at the symmetry plane. The highest amplitudes occur in the resonator volume.

4.1.5. Additively manufactured damped LOX throttle plate

The resonators were most easily integrated into the BKD injector head by replacing the throttle plate with a new version. The throttle plate is mounted inside the LOX manifold and contains throttling orifices which define the inlet geometry to the LOX posts. The existing throttle plates of the experiment were machined conventionally. The most cost effective way to produce the damped throttle plate, including 40 small-scale Helmholtz resonators with seven different designs, was via additive manufacturing, specifically selective laser melting (SLM) of stainless steel (316L or 1.4404). In order to achieve good comparability to the existing throttles, surface finishing was applied. A conventional drilling process was used to realize the correct throttle diameter with low tolerance and a smooth surface. Also wire cutting has been applied in order to reduce the surface roughness of the end face of the plate. Fig. 9 shows the throttle plate after the surface finishing. The different Helmholtz resonators of the three injector rows are visible. The dimensions of the Helmholtz resonator volumes and channels were within the common state-of-the-art accuracy of SLM manufacturing. Also the small purging hole diameters of 0.4 mm could be realized.

In a full scale rocket engine the injector head typically consists of hundreds of injector elements. Manufacturing injector heads additively has the potential to drastically reduce the number of parts and costs. In Europe, studies have been published on SLM production of an upper stage injector head [28,29]. Parts of the Japanese LE-9 engine are produced by SLM [30]. Implementing the intricate geometries of the acoustic dampers into the injectors could easily be realized in an additively manufactured injector head.

4.2. Operating conditions

In order to test the effectiveness of the new damping device, the test sequence in Fig. 10 was realized. The sequence comprises two p_{cc} stages of 80 bar and 70 bar, and during each pressure stage the mixture ratio ROF was ramped from 4 to 6. The hydrogen injection temperature (T_{H2}) was kept constant at around 100 K. Under these conditions the thermal power reaches around 90 MW and the thrust around 24 kN, which makes BKD comparable to small upper-stage engines.

Two load points (LP), labelled LP1 and LP2 in Fig. 10, were analyzed from the test data. The first is defined by a p_{cc} of 80 bar and ROF of 6, and the second is with 70 bar and ROF 6, which correspond to the most unstable conditions studied previously by Groening [10,26]. This makes them best suited to verify the function of the damping device in reducing the impact of injection-coupled instability.

4.3. Measurement technique

Due to the representative, harsh conditions inside the combustor it is only possible to have flush-mounted dynamic pressure sensors in the measurement ring, which is mounted close to the injection plane and is shown in Fig. 11. Eight dynamic pressure sensors and four fibre-optical probes are distributed circumferentially in the main measurement plane 5.5 mm downstream of the faceplate. The pressure oscillation signals are recorded with a sampling rate of 100 kHz and a 30 kHz anti-aliasing filter is applied. The measurement range of the sensors is ± 30 bar.

The fibre-optical probes contain a sapphire rod and the flame radiation is transferred to photomultipliers (PM) by optical fibers. Interference filters for the OH* emission with a center wavelength of 310 nm and a full width at half-maximum of 10 nm are mounted in front of the PMs. The signals are also recorded with 100 kHz. The full acceptance angle of the probes is less than 2. This feature has been used to align the optical probes to specific injectors [10]. As indicated in Fig. 11 PM1 is aligned with an injector of the inner ring and PM2–PM4 with outer ring injectors.

In the test run with the damped throttle plate, the flame observed by PM1 should be damped around 20 kHz, while PM3 and PM4 are directed at outer row injectors which are tuned to damp the 2L post mode (10 kHz), respectively. For comparison, PM2 is aligned with one of the two undamped injectors of the outer row.

5. Results and discussion

In order to be a potential solution for future rocket engines, the device should reduce injection-driven heat release oscillations without negative effects on important engine parameters such as the combustion efficiency or the injection pressure drop. The test data were therefore analyzed for all these aspects and the results are described in this chapter.

5.1. Flame dynamics with damped injectors

First, the effectiveness of the device in reducing injection-driven heat release oscillations was assessed. The level of flame oscillation is inferred by the dynamic content of the optical probe signals. The signals are normalized by their mean value ($I'/\bar{I}$) for comparability between the four optical probes.

The normalized intensity oscillations of another test run with a similar mxiture ratio ramping sequence and the standard, undamped injectors were analyzed first. The top graph of Fig. 12 shows the Power Spectral Density (PSD) of the normalized PM2 signal for the load point of 80 bar ROF 6 (similar to LP1 in Fig. 10). The optical probe PM2 is defined as the reference signal for the following analysis. The middle graph of Fig. 12 shows the PSDs of the remaining outer row PMs. In all three PSDs dominant peaks at multiples of 5 kHz can be observed, which are the resonant frequencies of the LOX posts [10]. It seems that all three outer row optical probe signals show consistent oscillation amplitudes.

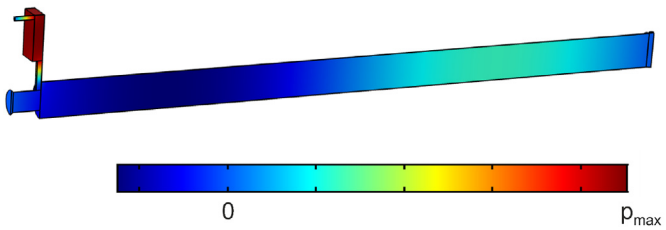

Fig. 8. Acoustic pressure distribution of LOX post 2L mode of a damped injector.

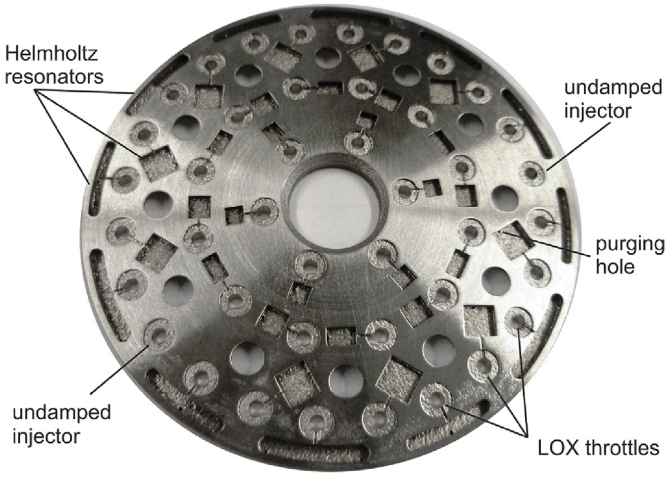

Fig. 9. Photo of 3D printed BKD LOX post throttle plate with acoustic absorbers.

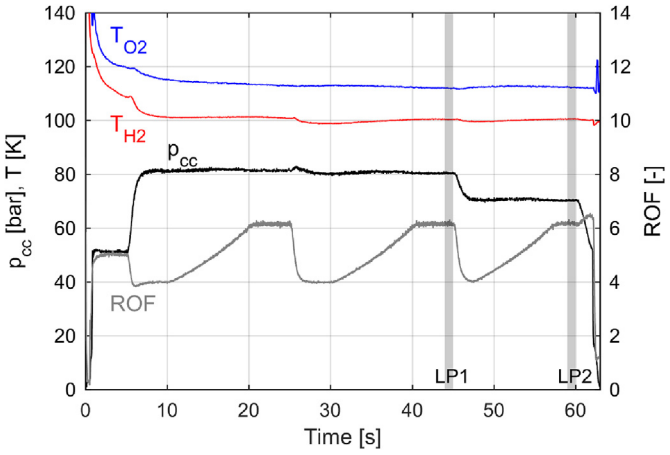

Fig. 10. Test sequence of the investigated test run with damped injectors.

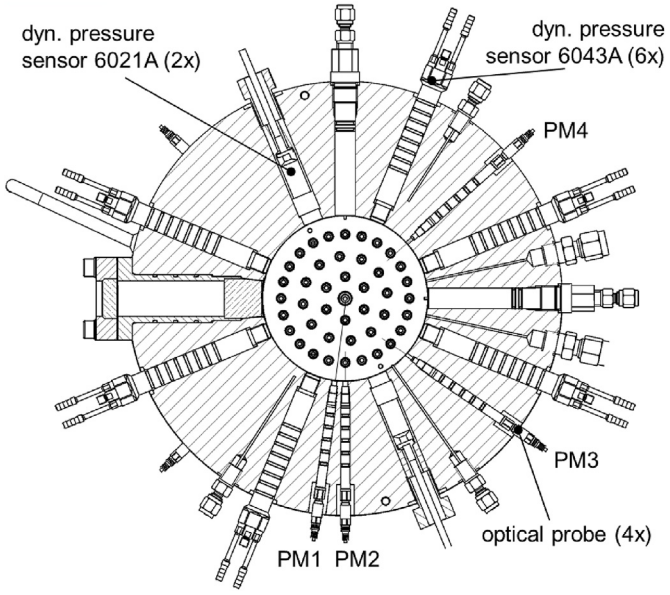

Fig. 11. Positions of the optical probes in the measurement ring with respect to the injector pattern.

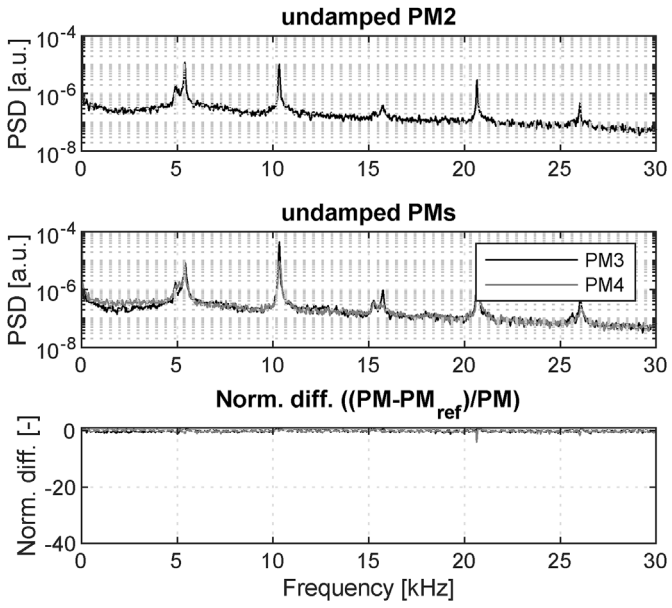

Fig. 12. PSDs of normalized PM signals of outer row injectors for LP1 (80 bar ROF 6) with the standard injectors. Also the normalized difference of the spectras to the reference PM2 is shown.

However, in the logarithmic scale of the PSDs it is difficult to distinguish the exact peak heights. For that reason, the bottom graph of Fig. 12 shows the normalized difference of the PSDs to the reference PM2, e.g. (PM3-PM2)/PM3. The linear scale difference shows a value close to zero over all frequencies and indicates that all the outer row PMs show very similar flame response to the excited injector acoustics. Therefore it is concluded that the locations of the optical probes in the measurement ring have no influence on $I'/\bar{I}$.

Fig. 13 shows the PM PSDs for the same operating condition of 80 bar ROF 6 for the run with the damped injectors. The top graph again shows the PSD of the undamped reference PM2. The 2 p.m. signals of flames which have the 2L post mode damped at 10 kHz can be

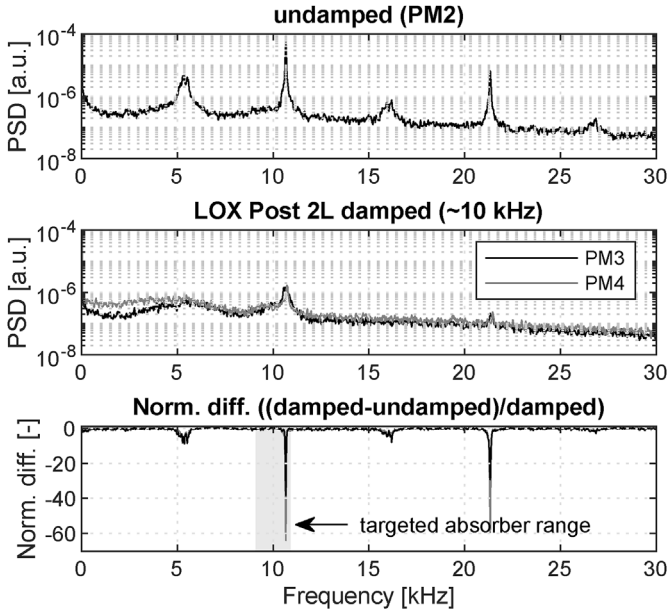

Fig. 13. PSDs of normalized PM signals of outer row injectors (PM2, top) for LP1 (80 bar ROF 6) with the damped injectors (PM3, PM4, middle). The normalized difference of the spectra from damped to the undamped reference PM2 is also shown (bottom).

found in the center plot and show a significant reduction in amplitude for all LOX post modes. The linear normalized difference of the two outer row injectors to the undamped reference PM2 is shown in the lower graph of Fig. 13. The dampers worked very efficiently in reducing the 10 kHz oscillation of the flames. The PSD peak height was reduced by a factor of more than 60. A strong impact on the first harmonic overtone at 20 kHz was also observed. It is currently unclear why the dampers also had an effect on the 1L and 3L modes of the LOX posts at about 5 and 15 kHz, respectively.

Fig. 14 shows the same plots for the inner row injector, which is damped on the 4L mode (PM1). Here, a difference of almost zero is present for the 2L mode around 10 kHz, whereas at 20 kHz the dampers reduced the OH* oscillations of the flame by a factor of 3.

The operating condition of 80 bar ROF 6 showed the best interaction between the LOX post 2L and chamber 1T mode in previous investigations. Gröning also defined the load point of $p_{cc} = 70$ bar ROF 6 (LP2 in Fig. 10) as semi-unstable [26]. The PSDs and difference to PM2 for outer row injectors are presented in Fig. 15. Again the flame dynamics are strongly reduced for the damped injectors of the outer row. The inner row injector is not shown here, but it shows similar oscillation amplitudes as the undamped flame up to the 3L mode around 15 kHz, and the 20 kHz peak is reduced by more than 60%.

5.2. Influence of damped injectors on pressure oscillations

Theoretically, the reduced flame oscillations should lead to lower amplitudes of the 1T mode in the chamber. The pressure oscillations in the chamber for the two different runs were compared. Fig. 16 shows the spectrogram of chamber pressure oscillations for the test run with the standard injectors. A driving of the 1T mode for some operating conditions can clearly be observed.

In comparison, Fig. 17 shows the same spectrogram for the run with damped injectors. First it can be seen that the test sequence and the propellant temperatures were very similar to the undamped run. The spectrogram in this run shows a reduction of the 1T oscillation amplitudes.

A more direct assessment of acoustic amplitude reduction can be made by comparing PSDs as was done previously for the optical probe signals. Fig. 18 shows an averaged PSD of all p' sensors in the chamber for the previously unstable operating condition of 80 bar and ROF 6. It is compared with those from both runs with the standard injectors and the damped LOX posts. As can be seen, the amplitude of the 1T mode peak at 10 kHz was significantly reduced in the test with the damped injectors.

5.3. Influence of the dampers on injection pressure drop

One of the important characteristics of an injector is the pressure drop (Δp_{inj}). On the one hand it has to be large enough to prevent feed system coupling leading to chugging and on the other hand as low as possible in order to reduce the maximum system pressure and the required power to drive the turbomachinery. For the operating condition of 80 bar and ROF 6, the LOX injection pressure drop with the damped injectors was 12.7% of p_{cc}, which is representative of real engines. The injector pressure loss was defined as

$$\Delta p_{inj} = p_{O2} - p_{cc} = \zeta \frac{\rho u^2}{2} \tag{4}$$

where u is the velocity in the posts and ζ the pressure loss coefficient of the LOX injector. The ζ values for different throttle plates over various operating conditions was compared.

The calculated ζ value of the damped throttles over the whole run was 1.21 ± 0.14. In comparison, the ζ values for four other existing BKD throttle plates without dampers varied between 1 and 1.6 with a mean value averaged over 14 test runs of 1.257. This indicates that other factors, such as slight differences between the orifices due to manufacturing tolerances, have a larger impact on the injection pressure drop than the resonators in the new throttle plate. Therefore, the acoustic dampers in the LOX posts have no negative effect on Δp_{inj}.

5.4. Influence of the dampers on combustion efficiency

Another important aspect of injector design is its influence on combustion efficiency. In rocket engine analysis, combustion performance is often evaluated by the value of characteristic velocity,

$$c* = \frac{p_{cc} A_t}{\dot{m}}. \tag{5}$$

The $c*$ was evaluated for the chamber pressures of 70 and 80 bar and mixture ratios from 4 to 6. Fig. 19 shows the calculated $c*$ values for the standard configuration and the damped injectors in comparison. The error bars were calculated with Gaussian error propagation and show the measurement uncertainties in the mass flow meters and the pressure sensors. As can be seen, there is no measurable loss of performance due to the damped injectors.

6. Conclusions

Within the framework of this study, a new damping device to prevent injection-coupled combustion instabilities in liquid propellant rocket engines has been introduced and tested on a representative research combustion chamber. This new damping method is characterized by acoustic resonators, which are connected to the injector tubes. Instead of damping the pressure oscillation of the instability in the chamber, the resonators are tuned on the acoustic modes of the injection elements. To the author's knowledge this study presents the first damping device which aims at reducing the driving source of high-frequency combustion instabilities rather than the resulting chamber pressure oscillations.

A main design feature of the device are small diameter purging holes which connect the resonator volumes with the injector manifold. This ensures the same speed of sound in the resonators and the injectors. This characteristic simplifies tuning of the resonators. In

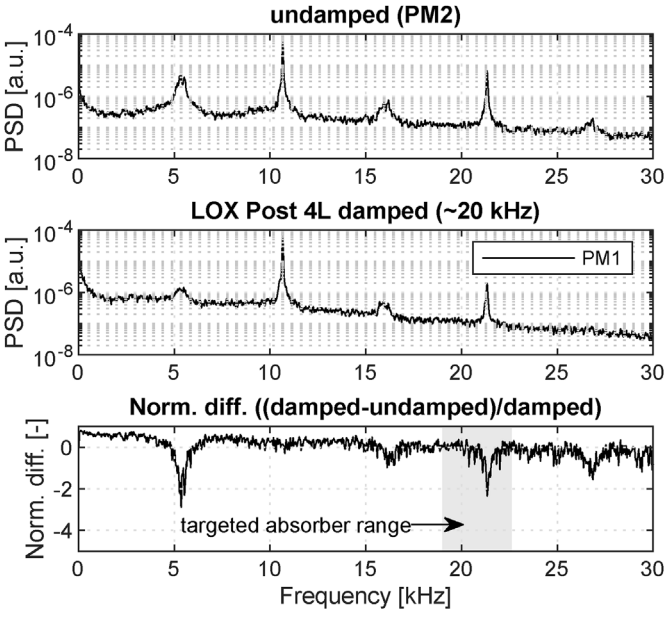

Fig. 14. PSDs of normalized PM signals of outer row (PM2, top) and inner row (PM1, middle) injectors for LP1 (80 bar ROF 6) with the damped injectors. The normalized difference of the PM1 spectrum to the undamped reference PM2 is also shown (bottom).

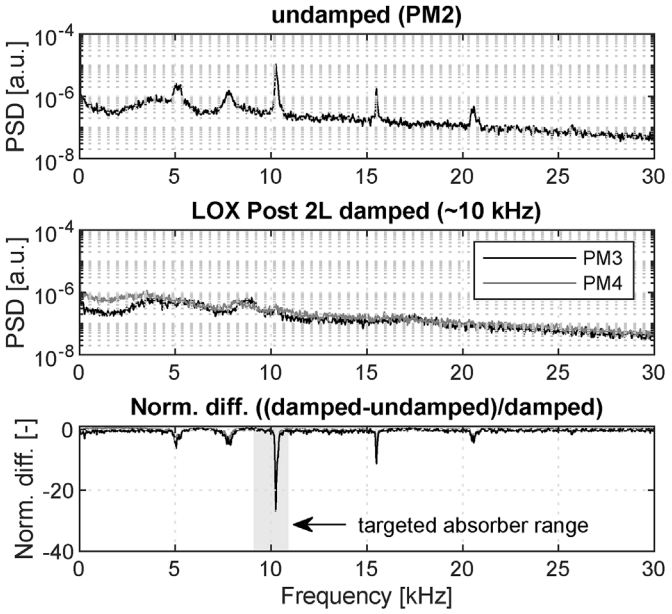

Fig. 15. PSDs of normalized PM signals of outer row injectors for LP2 (70 bar ROF 6) with the damped injectors. The normalized difference of the spectra to the undamped reference PM2 is also shown (bottom).

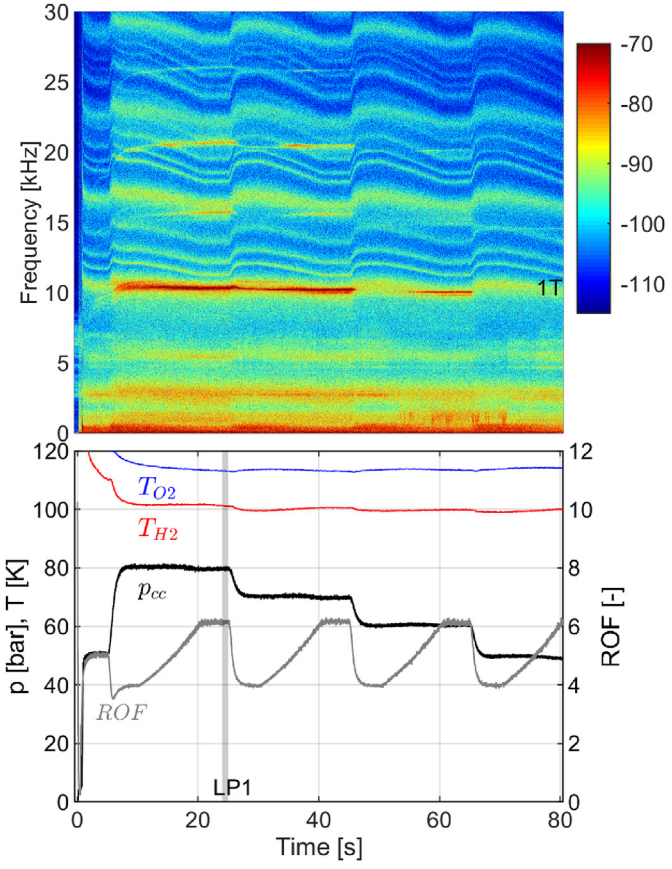

Fig. 16. Test sequence and acoustic pressure sensor spectrogram of a BKD test run with the standard (undamped) injectors.

addition, once accurately tuned, the resonators damp the injector acoustics for all operating conditions.

The performance of the damping device was investigated experimentally. Measurements from test runs with the new injector damping device installed were compared with test runs with the original injector

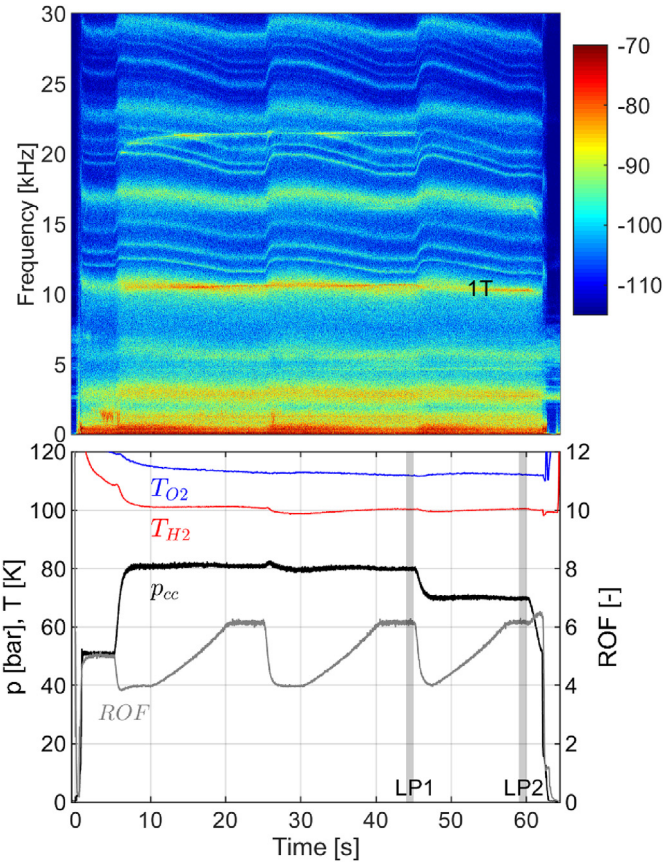

Fig. 17. Test sequence and acoustic pressure sensor spectrogram of a BKD test run with the damped LOX injectors.

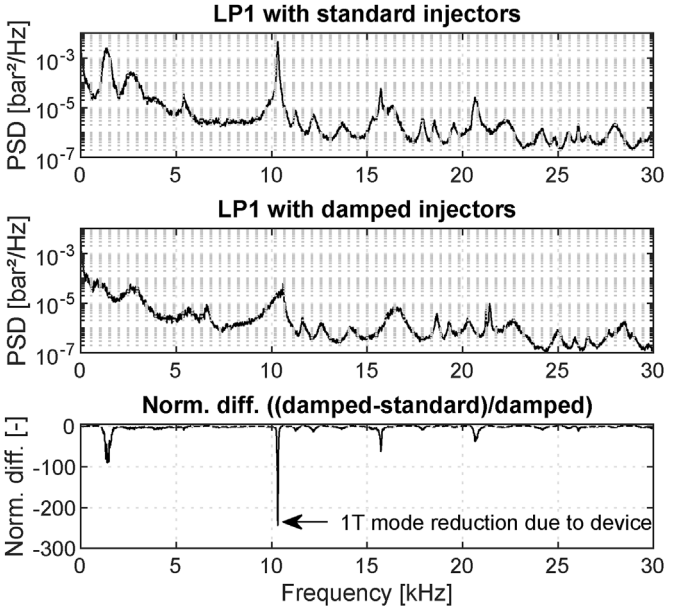

Fig. 18. Comparison of acoustic pressure PSD for the load point 80 bar ROF 6 with standard injectors and damped injectors.

design. The flame dynamics were analyzed by means of flame radiation fluctuations and showed that dominant modes with the resonant frequencies of the oxidizer posts were reduced significantly by the damping device. It was shown that the device had no negative effect on important injector characteristics.

In summary, the main injection characteristics, as well as the

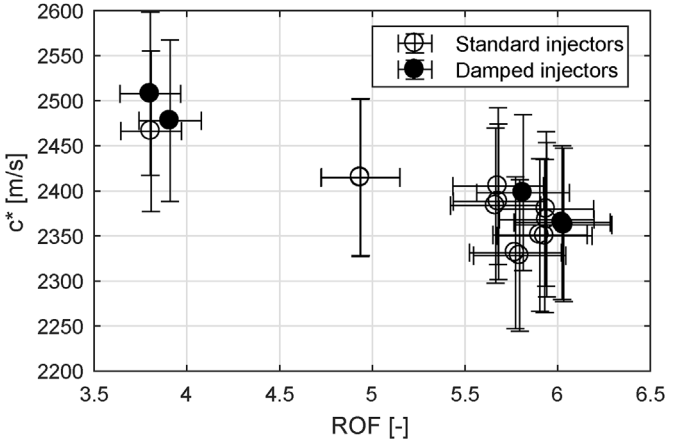

Fig. 19. Comparison of combustion performance between normal and damped injectors for chamber pressures of 70–80 bar.

injector dimensions were effectively unchanged, while flame dynamics, which led to combustion instabilities in past campaigns, were reduced.

Injector-coupling has been observed for a number of sub-scale experiments up to full scale engines, and is a rather common source of combustion instabilities in cryogenic rocket engines using shear coaxial injection elements. The device presented in this work is also expected to be applicable to full-scale engines to reduce the risk of combustion instabilities.

Acknowledgments

Financial support has been provided by the German Research Foundation (Deutsche Forschungsgemeinschaft – DFG) in the framework of the Sonderforschungsbereich Transregio 40. The authors would like to thank the crew of the P8 test bench as well as Alex Grebe for their assistance in performing the test runs.

References

[1] D. Harrje, F. Reardon (Eds.), Liquid Propellant Rocket Combustion Instability, NASA SP-194, 1972.
[2] J.C. Oefelein, V. Yang, Comprehensive review of liquid-propellant combustion instabilities in F-1 engines, J. Propuls. Power 9 (5) (1993) 657–677, https://doi.org/10.2514/3.23674.
[3] D. Watanabe, H. Manako, T. Onga, T. Tamura, K. Ikeda, M. Isono, Combustion stability improvement of LE-9 engine for booster stage of H3 launch vehicle, Mitsubishi Heavy Ind. Tech. Rev. 53 (2016) 28–35.
[4] Y. Fukushima, H. Nakatsuzi, R. Nagao, K. Kishimoto, K. Hasegawa, T. Koganezawa, S. Warashina, Development status of LE-7A and LE-5B engines for H-IIA familiy, Acta Astronaut. 50 (2002) 275–284.
[5] B. Wang, H. Zhang, J. QinG.Y., On triggering and suppresion of combustion instabilities in LOX/RP-1 LREs, Thermoacoustic Instabilities in Gas Turbines and Rocket Engnines: Industry Meets Academia, Paper No: GTRE-001, Munich, Germany, 2016.
[6] G. Langel, E. Laudien, R. Pongratz, Combustion stability characteristics of the Ariane 5 L7 engine, 42nd Congress of the International Astronautical Federation, Paper Number: IAF-91-250, Montreal, Canada, 1991.
[7] J.P. Dutheil, D.G. Langel, Ariane 5 upper-stage ignition conditions improvement, and return to operation with "envisat" payload, Acta Astronaut. 53 (2003) 585–595.
[8] D. Preclik, P. Spagna, Low Frequency and High Frequency Combustion Oscillation Phenomena inside a Rocket Combustion Chamber Fed by Liquid or Gaseous Propellants, AGARD, Combustion Instabilities in Liquid-Fueled Propulsion Systems, (1989).
[9] Y. Nunome, T. Onodera, M. Sasaki, T. Tomita, K. Kobayashi, Y. Daimon, Combustion instability phenomena observed during cryogenic hydrogen injection temperature ramping tests for single coaxial injector elements, 47th AIAA/ASME/SAE/ASEE Joint Propulsion Conference & Exhibit 2011, AIAA Paper 2011-6027, San Diego, California, 2011, https://doi.org/10.2514/6.2011-6027.
[10] S. Gröning, J.S. Hardi, D. Suslov, M. Oschwald, Injector-driven combustion instabilities in a Hydrogen/Oxygen rocket combustor, J. Propuls. Power 32 (3) (2016) 560–573, https://doi.org/10.2514/1.B35768.
[11] H. Kawashima, K. Kobayashi, T. Tomita, A combustion instability phenomenon on a LOX/Methane subscale combustor, 46th AIAA/ASME/SAE/ASEE Joint Propulsion Conference & Exhibit 2010, AIAA Paper 2010-7082, Nashville, Tennessee, 2010, https://doi.org/10.2514/6.2010-7082.
[12] J.C. Melcher, R.L. Morehead, Combustion stability characteristics of the project morpheus liquid oxygen/liquid methane main engine, 50th AIAA/ASME/SAE/ASEE Joint Propulsion Conference & Exhibit 2014, AIAA Paper 2014-3681, Cleveland, Ohio, 2014, https://doi.org/10.2514/6.2014-3681.
[13] R.J. Jensen, H.C. Dodson, S.E. Claflin, LOX/Hydrocarbon Combustion Intability Investigation, NASA CR 182249, NASA Lewis Research Center, 1989.
[14] G.P. Sutton, O. Biblarz, Rocket Propulsion Elements, eighth ed., John Wiley & Sons, New York, 2010.
[15] J.W.S. Rayleigh, The explanation of certain acoustical phenomena, Nature 18 (455) (1878) 319–321.
[16] B.T. Zinn, Pulse combustion: recent applications and research issues, Symposium (International) on Combustion, 24 1992, pp. 1297–1305, , https://doi.org/10.1016/S0082-0784(06)80151-7 (1).
[17] S. Webster, Analysis of Pressure Dynamics, Forced Excitation and Damping in a High Pressure LOX/H2 Combustor, Ph.D. thesis RWTH Aachen, Aachen, Germany, 2016.
[18] H.J. Dennis, J. Hutt, T. Nesman, Stability testing of a modified space shuttle main engine, 27th Joint Propulsion Conference, Sacramento, CA, 1991, https://doi.org/10.2514/6.1991-1983.
[19] W. Wang, D. Zheng, G. Qiao, Development status of the cryogenic oxygen hydrogen YF-77 engine for long-march 5, 64th International Astronautical Congress (IAC), Paper Number = IAC-13,C4,1,2,x17679, Beijing, China, 2013.
[20] M.L. Dranovsky (Ed.), Combustion instabilities in liquid rocket engines: testing and development practices in Russia, Progress in Astronautics and Aeronautics. American Institute of Aeronautics and Astronautics, Vol. 221 2007.
[21] E. Laudien, R. Pongratz, R. Pierro, D. Preclik, Experimental procedures aiding the design of acoustic cavities, in: V. Yang, W.E. Anderson (Eds.), Liquid Rocket Engine Combustion Instability, Ch. 14 American Institute of Aeronautics and Astronautics, Washington, DC, 1995, pp. 377–399.
[22] J.J. Hutt, M. Rocker, High-frequency injection-coupled combustion instability, in: V. Yang, W.E. Anderson (Eds.), Liquid Rocket Engine Combustion Instability, Ch. 12 American Institute of Aeronautics and Astronautics, Washington, DC, 1995, pp. 345–356.
[23] S. Gröning, J.S. Hardi, D. Suslov, M. Oschwald, Influence of hydrogen temperature on the stability of a rocket engine combustor operated with hydrogen and oxygen, CEAS Space J. 9 (1) (2017) 59–76, https://doi.org/10.1007/s12567-016-0130-8.
[24] C. Bourquard, N. Noiray, Criteria for choosing helmholtz or quarter-wave dampers to suppress combustion instabilities, Thermoacoustic Instabilities in Gas Turbines and Rocket Engnines: Industry Meets Academia 2016, Munich, Germany, 2016, https://doi.org/10.3929/ethz-a-010722919.
[25] W. Armbruster, J.S. Hardi, D. Suslov, M. Oschwald, Injector-driven flame dynamics in a high-pressure multi-element oxygen-hydrogen rocket thrust chamber, J. Propuls. Power 35 (2019) 632–644, https://doi.org/10.2514/1.B37406.
[26] S. Gröning, Untersuchung selbsterregter verbrennungsinstabilitäten in einer raketenbrennkammer, Ph.D. thesis RWTH Aachen, Aachen, Germany, 2017.
[27] E.W. Lemmon, M.L. Huber, M.O. McLinden, NIST Standard Database 23. NIST Reference Fluid Thermodynamic and Transport Properties–REFPROP, (2013) version 9.1.
[28] S. Soller, R. Behr, S. Beyer, F. Laithier, M. Lehmann, A. Preuss, R. Salapete, Design and tesing of liquid propellant injectors for additive manufacturing, 7th European Conference for Aeronautics and Aerospace Sciences, EUCASS), Milano, Italy, 2017, , https://doi.org/10.13009/EUCASS2017-306.
[29] T. Fuhrmann, B. Mewes, F.D. Moya, M. Horstmann, Flpp etid: enabling technologies for future european upper stage engines, 7th European Conference for Aeronautics and Aerospace Sciences, EUCASS) 2017, Milano, Italy, 2017, , https://doi.org/10.13009/EUCASS2017-131.
[30] H. Kawashima, T. Kobayashi, K. Okita, Progress of LE-9 engine development, AIAA Propulsion and Engery Forum, 2018 Joint Propulsion Conference, AIAA Paper 2018-4458, Cincinnati, Ohio, 2018, https://doi.org/10.2514/6.2018-4458.